A New Approach for Power Signal Disturbances Classification Using Deep Convolutional Neural Networks

Yeong-Chin Chen, Sunneng Sandino Berutu, Long-Chen Hung, and Mariana Syamsudin
(Corresponding author: Yeong-Chin Chen)

Department of Computer Science and Information Engineering, Asia University
Taichung 41354, Taiwan
Email: ycchenster@gmail.com

(Received Jan. 25, 2021; Revised and Accepted May 12, 2022; First Online June 29, 2022)

Abstract

This paper proposes a new approach for power signal disturbances (PSDs) classification using a two-dimension (2D) deep convolutional neural network (CNN). The data preprocessing stage introduces a conversion method from signal to the 2D grayscale image. Firstly, the signal is divided into multiple cycles. The zero-crossing rate is adopted to specify a cycle's start and endpoints. Then, the cycles are transformed into matrices. Next, the matrices are merged into a new form matrix. Lastly, the matrix is converted into the 2D image grayscale. The obtained 2D image preserves information and waveform the sinusoidal of the signal. The experiment was carried out on datasets containing 14 different disturbance categories with the same model learning structure. The results show that the 2D deep CNN performs better than the one-dimension (1D) deep CNN. According to this result, the 2D deep CNN can improve the PSDs classification effectiveness. Furthermore, the proposed method outperforms the conversion method used in previous studies.

Keywords: 2D Deep CNN; Conversion; Image; Signal Disturbance

1 Introduction

Power quality refers to interference-free electricity signals. Various deviations caused from loads [11,18] are to be considered as power signal disturbances (PSDs). The emergence of distortions in the power quality strongly affects the decreasing performance or malfunction of electricity equipment at industry, office, and home. In addition, the disturbances can cause an economic loss because of the reparation and replacement cost of the equipment damage. Therefore, identifying and classifying the PSDs are the best method in those worst impact avoiding. Scientific research has been carried out to address this problem. The rapid advancement of the deep learning method has been implemented in the PSDs field. Convolutional neural network (CNN) has the most performance capability and is widely employed in the PSDs classification work [18]. The one-dimensional (1D) CNN and the two-dimensional (2D) CNN methods have been implemented in the PSDs field. The 1D CNN is applied for the 1D dataset, whereas the 2D CNN is fed by the 2D dataset. Recently, the most popular CNN in the PSDs classification task is the deep CNN method. This method has higher performance in comparison with the others [21].

The 1D CNN in PSDs classification has been implemented by many authors [1, 5, 15, 17, 20, 21]. These works have proposed new approaches to improve the classification performance such as addressed the over fitting problem [21], improved feature extraction [1, 17], and introduced a hybrid model [15]. The performance shortages such computational time and model size are tried to be solved by implementing data compression techniques in the data preprocessing [5, 20]. However, these investigations consumed a lot of original information in the compression process.

In the beginning, the CNN method was employed for the 2D image classification purpose [16]. The 2D CNN method can learn the diversity and complexity of image features [12]. When the 2D CNN is implemented for the PSDs classification task, the 2D dataset is required for this method. However, the power signal data is one-dimensional and represented in sinusoidal waveforms. Therefore, a data preprocessing is required to convert from the power signal to the 2D image. Various conversion techniques were carried out by authors in references [2–4, 9, 10, 13, 14, 22, 24, 25]. The author in [13] employed a trajectory matrix to produce a lag-covariance model as image of PSDs. In addition, the work in [4] utilized quadratic means to generate the disturbance image. The other studies in [2, 3, 22] adopted a space phasor diagram (SPD) to transform the sag disturbance into the image. Besides, the investigations in [9, 10, 25] utilized a matrix to transform the signal disturbance into the 2D image. The sampling points of signal are rearranged into a number rows and columns in the matrix, then convert the matrix into the gray-scale image. The works in [14, 24] adopted a scalogram and spectrogram analysis to represent the signal in the image. However, the transforming process has changed the original information totally [2, 3, 22], thus several important features are lost. The image size resulted in [14] is a large and the training time costly. In addition, the performance comparison of the 1D CNN and the 2D CNN models for the PSDs classification is unevaluated in the previous investigations.

In this study, a robust data preprocessing method is developed to convert from the signal to the 2D gray-scale image, where the image results can represent the sinusoidal waveform and preserve the original information. The 2D image obtained is used as the 2D dataset in the 2D deep CNN for the PSDs classification purpose. Moreover, the performance comparison of the 1D and 2D deep CNN models for PSDs classification is evaluated utilizing a confusion matrix method. In addition, to compare the efficacy of proposed conversion approach, the conversion methods [9, 10, 25] are implemented using same the 1D signal and same the 2D deep CNN architecture. The rest of this paper is organized as follows. First, Section 2 presents the material of this work and methods utilized for signal conversion and the PSDs classification. Section 3 shows the experimental result and discussion. Finally, conclusion and future study are explained in Section 4.

2 Material and Methods

In this section, first, the mathematical formula for generation of PSDs data is explained. Furthermore, the approach of conversion signal-to-image proposed is presented. Then, the deep CNN model structure is discussed.

2.1 Mathematical Formula of PSDs

With the limitation of the real PSDs data, this work employed the mathematical formulas [8, 20, 21] to generate the synthetic PSDs. In these equations, the IEEE-1159 standard parameter variations [7] are adopted. As presented in Table 1, this work utilizes 14 categories of disturbance signal.

The parameters value such as intensity (α), distortion of the transient (β), distortion of the flicker (λ), time (t_1 and t_2) are generated randomly to obtain the variety of each disturbance category. The fundamental frequency (f) is adjusted at 60 Hz, whereas the sampling frequency (fs) is 3200 Hz [17], the cycle numbers (Nc) is 11, the sampling points (Ns) is 586, and the amplitude (A) is set at 1. The synthetic signals produced for each category are 11,000 samples so that the total samples are 154,000.

2.2 The Signal to Image Conversion Approach

In this approach, the signal is divided into multiple cycles, where zero-crossing rate (ZCR) is utilized to determine the start and endpoints of cycles. The cycles are transformed into the matrices. The matrices are then merged to form a new matrix. The matrix result is converted to the 2D grayscale image. The advantage of this approach is that the image resolution can be reduced. The main steps of the proposed approach are depicted in Figure 1.

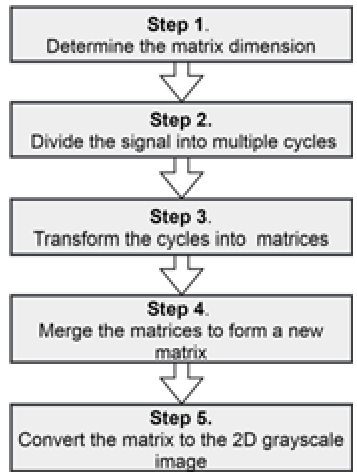

Figure 1: The steps of the conversion from the signal to the 2D grayscale image

The detailed explanation of Figure 1 is presented as follows:

Step 1. Determine the matrix dimension.

The square matrix (number of the rows (Nr) is equal to the number of the columns ($Ncol$) is chosen. The $Ncol$ is determined using Equation (1),

$$Ncol = ceiling(\frac{fs}{f}) \tag{1}$$

If fs and f values are 3200 and 60, respectively, so that $Ncol$ value is 54. Then, the matrix dimension is to be 54×54.

Step 2. Divide the signal into multiple cycles.

The signal is divided into 11 cycles, with the start and endpoints of each cycle determined by the ZCR. The rate at which the signal changes from negative to zero to positive is adopted in this work. As shown in Figure 2, the ZCR points obtained are marked in the signal.

According to Figure 2, the number of ZCR points obtained is 11, where the sampling points of the signal as ZCR are 1, 54, 107, 161, 214, 267, 320, 374, 427, 480, and 534. Therefore, the start and endpoints of each cycle can be obtained which presented in Table 2.

Table 1: Mathematical model and parameter of power signal disturbances

Categories	Mathematical formulas	Parameters
Normal	$y(t) = A[1 \pm \alpha(u(t-t_1) - u(t-t_2))]sin(\omega t)$	$\alpha \le 0.1$, $T \le t_2 - t_1 \le 9T$, $\omega = 2\pi f$
Sag	$y(t) = A[1 - \alpha(u(t-t_1) - u(t-t_2))]sin(\omega t)$	$0.1 \le \alpha \le 0.9$, $T \le t_2 - t_1 \le 9T$
Swell	$y(t) = A[1 + \alpha(u(t-t_1) - u(t-t_2))]sin(\omega t)$	$0.1 \le \alpha \le 0.8$, $T \le t_2 - t_1 \le 9T$
Interruption	$y(t) = A[1 - \alpha(u(t-t_1) - u(t-t_2))]sin(\omega t)$	$0.9 \le \alpha \le 1$, $T \le t_2 - t_1 \le 9T$
Harmonics	$y(t) = A[\alpha_1 sin(\omega t) + \alpha_3 sin(3\omega t) + \alpha_5 sin(5\omega t) + \alpha_7 sin(7\omega t)]$	$0.05 \le \alpha_3, \alpha_5, \alpha_7 \le 0.15$, $\sum \alpha_i^2 = 1$
Flicker	$y(t) = A[1 + \lambda sin(\omega_f t)]sin(\omega t)$	$8 \le f_f \le 25\ Hz$, $w_f = 2\pi f_f$ $0.05 \le \lambda \le 0.1$
Transient oscillation	$y(t) = A[sin(\omega t) + \beta e^{-(t-t_1)/\tau} sin(\omega_n(t-t_1))(u(t-t_2) - u(t-t_1))]$	$300 \le f_n \le 900$, $\omega_n = 2\pi f_n$,$0.5T \le t_2 - t_1 \le \frac{Nc}{3.33}T$, $8\ ms \le \tau \le 40\ ms$, $0.1 \le \beta \le 0.8$
Periodic notch	$y(t) = sin(\omega t) - sign(sin(\omega t)) \times \{\sum_{n=0}^{9} k\ [u(t-(t_1 - sn)) - u(t-(t_2 - sn))]\}$	$0.01T \le t_2 - t_1 \le 0.05T$, $t_2 \le s$, $t_1 \ge 0$, $0.1 \le k \le 0.4$, c={1,2,4,6}, $s = \frac{T}{c}$
Sag with harmonics	$y(t) = A[1 - \alpha(u(t-t_1) - u(t-t_2))][\alpha_1 sin(\omega t) + \alpha_3 sin(3\omega t) + \alpha_5 sin(5\omega t)]$	$0.1 \le \alpha \le 0.9$, $T \le t_2 - t_1 \le 9T$, $0.05 \le \alpha_3, \alpha_5, \alpha_7 \le 0.15$, $\sum \alpha_i^2 = 1$
Swell with harmonics	$y(t) = A[1 + \alpha(u(t-t_1) - u(t-t_2))][\alpha_1 sin(\omega t) + \alpha_3 sin(3\omega t) + \alpha_5 sin(5\omega t)]$	$0.1 \le \alpha \le 0.8$, $T \le t_2 - t_1 \le 9T$ $0.05 \le \alpha_3, \alpha_5, \alpha_7 \le 0.15$, $\sum \alpha_i^2 = 1$
Interruption with harmonics	$y(t) = A[1 - \alpha(u(t-t_1) - u(t-t_2))][\alpha_1 sin(\omega t) + \alpha_3 sin(3\omega t) + \alpha_5 sin(5\omega t)]$	$0.9 \le \alpha \le 1$, $T \le t_2 - t_1 \le 9T$ $0.05 \le \alpha_3, \alpha_5, \alpha_7 \le 0.15$, $\sum \alpha_i^2 = 1$
Flicker with harmonics	$y(t) = A[1 + \lambda sin(\omega_f t)][\alpha_1 sin(\omega t) + \alpha_3 sin(3\omega t) + \alpha_5 sin(5\omega t)]$	$0.05 \le \lambda \le 0.1$, $8 \le f_f \le 25\ Hz$, $0.05 \le \alpha_3, \alpha_5, \alpha_7 \le 0.15$, $\sum \alpha_i^2 = 1$
Flicker with sag	$y(t) = A[1 + \lambda sin(\omega_f t)(1 - \alpha(u(t-t_1) - u(t-t_2))]sin(\omega t)$	$0.1 \le \alpha \le 0.9$, $T \le t_2 - t_1 \le 9T$, $0.05 \le \lambda \le 0.1$, $8 \le f_f \le 25\ Hz$
Flicker with swell	$y(t) = A[1 + \lambda sin(\omega_f t)(1 + \alpha(u(t-t_1) - u(t-t_2))]sin(\omega t)$	$0.1 \le \alpha \le 0.8$, $T \le t_2 - t_1 \le 9T$, $0.05 \le \lambda \le 0.1$, $8 \le f_f \le 25\ Hz$

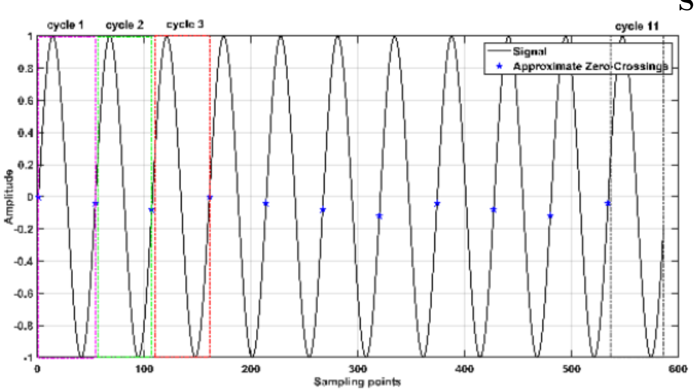

Figure 2: The zero-crossing rate points in the signal

Table 2: The start and endpoints of each cycle

Cycle	Start point	End point
1th	1	54
2nd	55	107
3rd	108	161
4th	162	214
5th	215	267
6th	268	320
7th	321	374
8th	375	427
9th	428	480
10th	481	534
11th	534	586

Step 3. Transform the cycles into matrices.

The cycle is transformed into a matrix of dimension 54×54. The start and the endpoints of the cycle are adopted as the columns of the matrix. In contrast, the sampling value of each point is used to determine the rows of the matrix. The sampling value of these points is then entered into the matrix elements. The following are the specifics:

1) Set the zero matrix:
   Initially, the elements of matrix are set at 0.

2) Indicate the column numbers:
   The start and endpoints of a cycle are indexed as column numbers to the matrix of dimension 54×54.

3) Arrange the sampling values into multiple classes:
   The sampling values of the signal are arranged into different classes. The number of classes should be the same as the number of rows, and the width of the classes should be the same as well. The width of the class interval (Int) is calculated with Equation (2). In this case, the row number refers to the class number.

$$Int = \frac{Hs - Ls}{Nr} \quad (2)$$

In which Hs represents the highest sampling value, whereas Ls represents lowest sampling value from all the sampling values. Furthermore, the lower (LB) and upper (UB) boundaries are used to define the class interval limits. The boundaries of each class are obtained through steps which depicted in Figure 3. The order of classes is started from the highest sampling value as the first class, while the lowest sampling value is in the 54rd class.

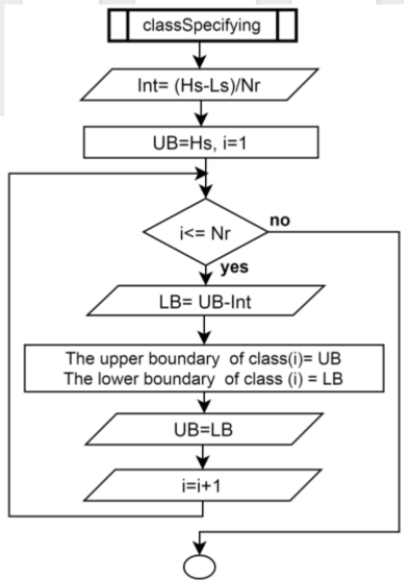

Figure 3: Steps of boundary determination for each classes

4) Specify the row numbers:
According to the classes resulted in Step 3.3, the row number of each sampling point can be obtained by comparing the sampling value to all the classes. The stages to determine the row number of each sampling point is presented in Figure 4.

5) Insert the sampling values of a cycle as the matrix elements:
The sampling values are inserted as the elements of matrix according to the row and column number which obtained at Steps 3.2 and 3.4.

Steps 3.1, 3.2, 3.4, and 3.5 are repeated to transform the rest cycles into the matrices.

Step 4. Merge the matrices to form a new matrix.
These matrices are combined by the add matrix function to form a new matrix with the same dimensions.

Step 5. Convert the matrix to the 2D grayscale image.
The elements of the matrix are converted to the grayscale color (0-255) to create the grayscale image. The image resolution result is 54×54 pixels.

2.3 Deep CNN Structure

The 1D and 2D of deep CNN methods were employed to classify the PSDs. The 1D convolution is utilized to classify the 1D signal, whereas the 2D convolution layer is implemented for the 2D image dataset. As depicted in Figure 5, the deep CNN structure is composed of 6

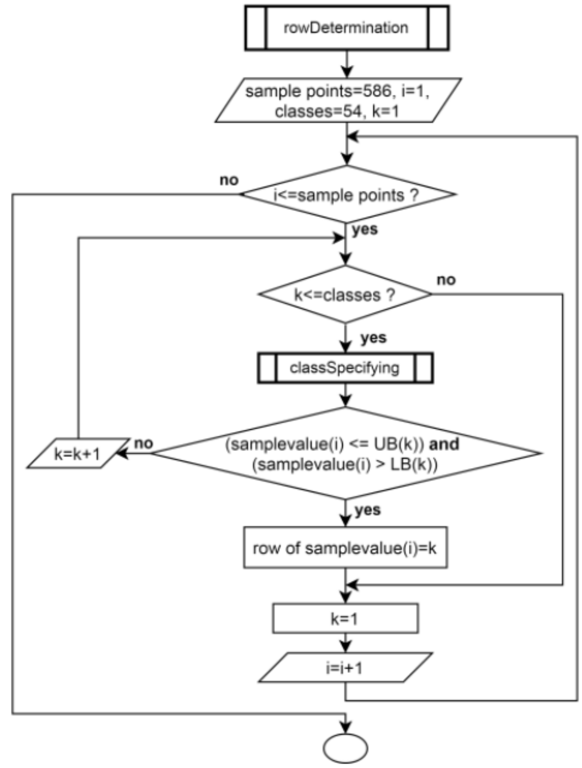

Figure 4: The steps of row specifying for each sampling point

convolution layers, 3 max pooling layers, a dropout layer, and 2 dense of fully connected layers. The detail of these compositions is presented in Table 3.

2.4 Model Evaluation

The confusion matrix is employed to measure the parameters such as accuracy, recall, precision, and f1-score [6, 19, 23]. The four categories output of the confusion matrix such as true positive (TP), false positive (FP), true negative (TN), and false negative (FP) are calculated to obtain these parameters values. The parameters are used to evaluate the classification performance of the 1D and 2D deep CNN models.

$$accuracy = \frac{TP+TN}{TP+TN+FP+FN} \quad (3)$$

$$recall = \frac{TP}{TP+FN} \quad (4)$$

$$precision = \frac{TP}{TP+FP} \quad (5)$$

$$f1-score = \frac{(2 \times precision \times recall)}{(precision+recall)} \quad (6)$$

3 Results and Discussion

In this section, first, the results of our approach for the signal to image conversion were presented. Then, the datasets used in this work are described. Furthermore,

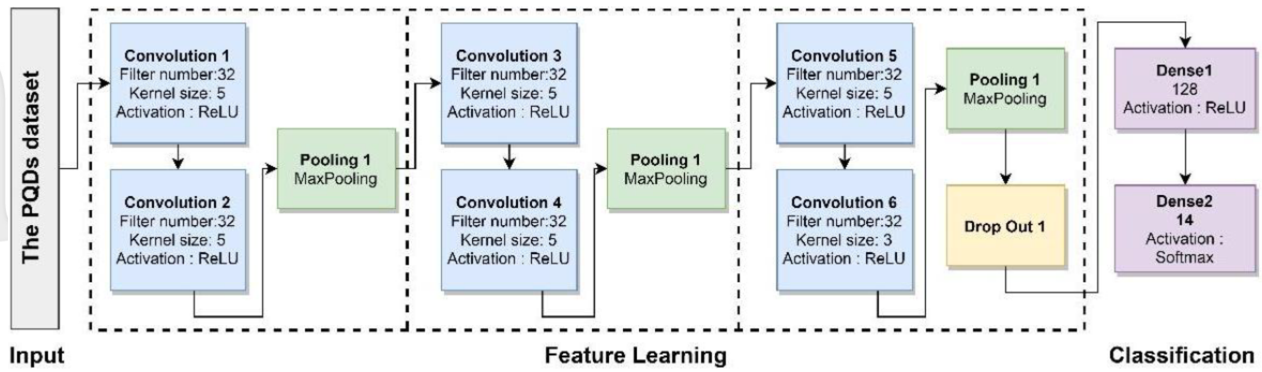

Figure 5: The architecture of the deep CNN model

the models training and testing stages are explained. The results of the training and testing are analyzed to evaluate the model's performance.

3.1 Implementation of the Signal to Image Conversion

The 14 synthetic disturbance types were generated using the mathematical model from Table 1. Then, the signal is converted to the 2D grayscale image utilizing our conversion proposed. As shown in Table 4, the 2D image obtained represents the sinusoidal waveform where the cycles of a signal are located in the image. In addition, the original amplitude values can be preserved in the image, although these values are converted into the grayscale color.

3.2 Datasets

In this work, the 1D signal dataset was obtained from the implementation result of the mathematical formula in Table 1, whereas the 2D image dataset was acquired from applying our approach for a conversion of the 1D signal to 2D image. In addition, we also employed the existing conversion methods [9, 10, 25] to obtain two 2D image datasets. Thus, three 2D image datasets are utilized in this work which presented in Table 5.

The 2D grayscale image sizes of the X, Y, and Z datasets are 54x54, 24 x 24, and 30 x 20, respectively. The 2D image dataset resulted from the previous methods are used to evaluate our approach performance. For the training and validation purpose, we used 9,900 samples per category, whereas about 500 samples of each type are utilized in the testing phase. The total samples of each dataset are 145,600. The details of dataset splitting for training, validation, and testing are presented in Table 6.

3.3 Training Stage Results

The model structure in Table 3 is utilized for the training phase. The 1D deep CNN model was trained using the 1D dataset, whereas the 2D deep CNN models were fed using the X, Y, and Z datasets. In the models, an Adam optimizer with a learning rate of 0.001 is adopted. Whereas, a categorical cross-entropy is employed for the loss function. In addition, the batch size is adjusted at 32. In the 2D deep CNN models, a rescaling layer is set at the first layer in the structure. Furthermore, a Nvidia Tesla T4 GPU accelerator 16 GB memory, and Intel Xeon (R) Central Processing Unit (CPU) @ 2.20 GHz are the training model environments.

In the beginning, the models were trained at 100 epochs. However, the accuracy and loss values of training and validation after the 50 epoch are shown unstable. Therefore, the models were retrained at 50 epochs. In addition, the dropout layer values of each model are adjusted to achieve the fitting accuracy and loss values between training and validation in the models. The dropout values for the 1D deep CNN, the 2D deep CNN X, the 2D deep CNN Y, and the 2D deep CNN Z are set at 0.55, 0.37, 0.45, and 0.55, respectively. Finally, the evaluation of the performance model training of the 1D and 2D deep CNN presents in Table 7. The fitting graph between the training and validation of models are displayed in Figure 6.

As presented in Table 7, generally, the performance of the 1D deep CNN outperforms both in the accuracy of training and validation than the 2D deep CNN models. In addition, the validation accuracy values are a higher than the training accuracy for all models. In the 2D deep CNN, the accuracy value of the 2D deep CNN X model exceeds the others. It indicates that the proposed approach performance in the conversion task is better than the previous approaches.

3.4 Discussion

In the models evaluation stage, the 1D deep CNN was tested using 7,000 samples of the 1D signal, whereas the 2D deep CNN models were examined with 7,000 samples each which were obtained from our approach, the author's method in [9, 10], and in [25]. The results of each model testing are presented in the confusion matrices which are shown in Figure 7. From these confusion matrices, the parameters value such the recall, the precision, and the

Table 3: The detail of model architecture

Layer	The 1D deep CNN	The 2D deep CNN
Convolution 1	Conv1D (32,5), activation = rectified linier unit (ReLU)	Conv2D (32,5) , activation=ReLU
Convolution 2	Conv1D (32,5) , activation=ReLU	Conv2D (32,5) , activation=ReLU
Pooling 1	Maxpooling1D(2)	Maxpooling2D(2)
Convolution 3	Conv1D (32,5) , activation=ReLU	Conv2D (32,5) , activation=ReLU
Convolution 4	Conv1D (32,5) , activation=ReLU	Conv2D (32,5) , activation=ReLU
Pooling 2	Maxpooling1D(2)	Maxpooling2D(2)
Convolution 5	Conv1D (32,5) , activation=ReLU	Conv2D (32,5) , activation=ReLU
Convolution 6	Conv1D (32,5) , activation=ReLU	Conv2D (32,5) , activation=ReLU
Pooling 3	Maxpooling1D(2)	Maxpooling2D(2)
Dense 1	Units = 128, activation=ReLU	Units = 128, activation=ReLU
Dense 2	Units = 14, activation= softmax	Units = 14, activation= softmax

Table 4: Representation of the 1D signal and the 2D image

Disturbance type	1D signal	2D grayscale image	Disturbance type	1D signal	2D grayscale image
Normal	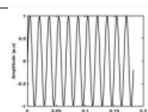		Sag wit harmonics	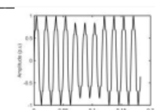	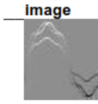
Flicker	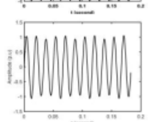		Swell with harmonics	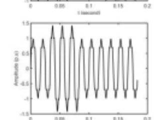	
Harmonics	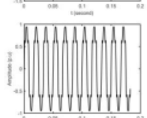		Interruption with harmonics	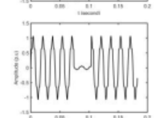	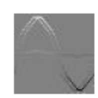
Interruption	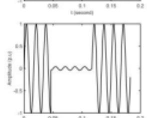		Flicker with harmonics	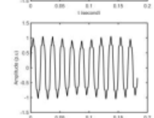	
Notch	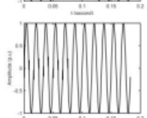		Flicker with sag	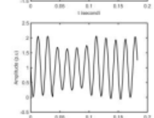	
Sag	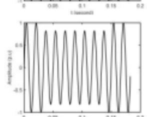		Flicker with swell	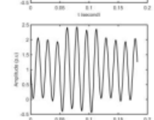	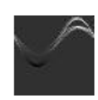
Swell	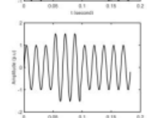		Transient	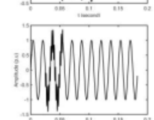	

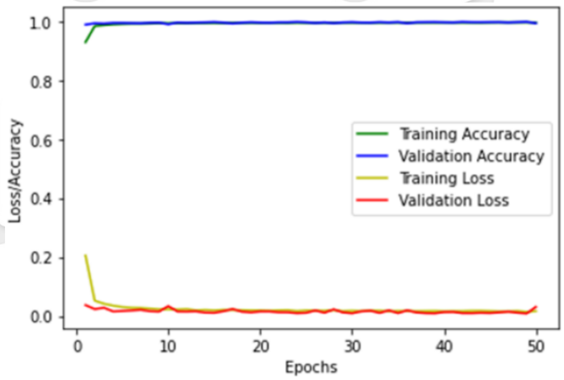

(a)

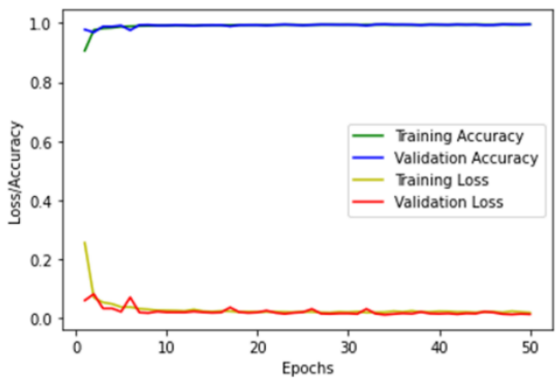

(b)

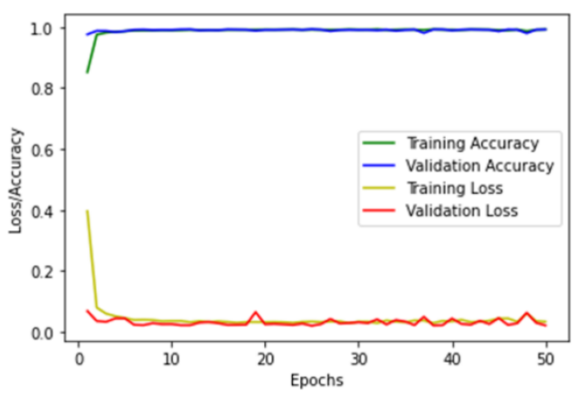

(c)

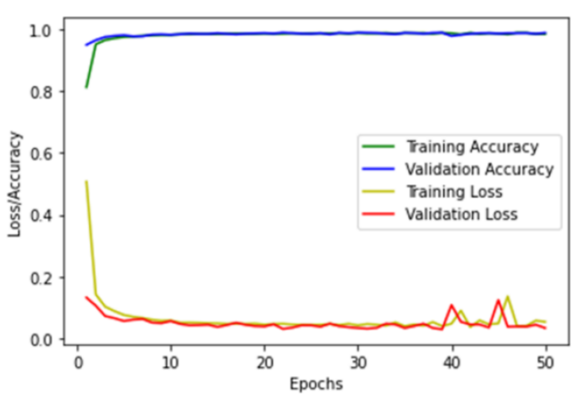

(d)

Figure 6: Fitting model of (a). the 1D deep CNN, (b). the 2D deep CNN X, (c). the 2D deep CNN Y, (d). the 2D deep CNN Z

Table 5: The 2D dataset and model name

Conversion method	Dataset	Model
Our proposed approach	X	2D deep CNN X
Author's approach [9,10]	Y	2D deep CNN Y
Author's approach [25]	Z	2D deep CNN Z

Table 6: Splitting of the 1D and 2D dataset

	1D signal	2D grayscale image
Training set	110,880	110,880
Validation set	27,720	27,720
Testing set	7,000	7,000

Table 7: Models performance in the training phase

Models Models	Training accuracy (%)	Validation accuracy (%)
1D deep CNN	99.27	99.51
2D deep CNN X	99.10	99.23
2D deep CNN Y	98.68	98.91
2D deep CNN Z	97.97	98.33

f1- score are obtained.

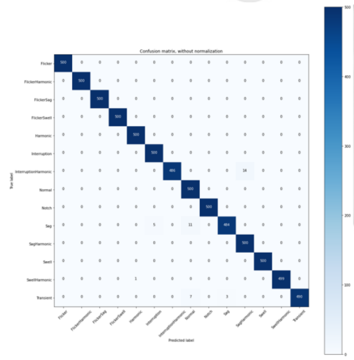

(a)

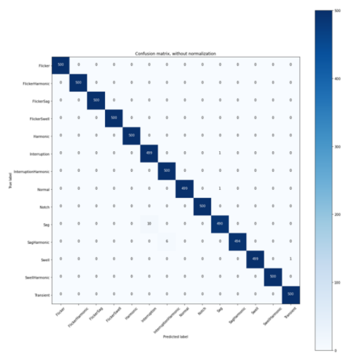

(b)

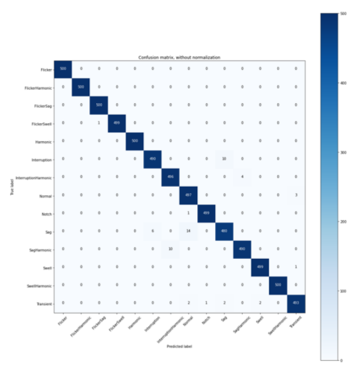

(c)

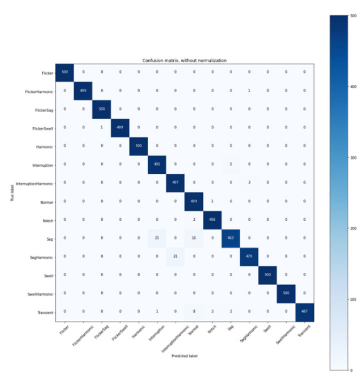

(d)

Figure 7: Confusion matrix of (a). the 1D deep CNN, (b). the 2D deep CNN X model, (c). the 2D deep CNN model, (d). the 2D deep CNN Z model

Firstly, we evaluated the testing performance of the 1D deep CNN and the 2D deep CNN X models. The parameters value of each disturbance are presented in Table 8 and Figure 8. The experiment's result showed that the flicker category and its combination achieved 100% for all the parameters value of both the models. These results are also obtained by the authors in [5, 21]. As the confusion matrices presented in Figure 7(a) and 8(b), the testing resulted of the 1D deep CNN, the number of disturbances in which the TP values reaching 100% are ten categories, whereas the 2D deep CNN X obtains nine categories. On the other hand, the lowest TP value of the 1D deep CNN is the interruption harmonic at 97.2%, where the rest (FN) is detected as the sag harmonic. Meanwhile, in the 2D deep CNN X model, the sag category is the lowest with 98%, where the rest (FN) is identified as the interruption disturbance. It can occur because the minimum boundary value of the intensity (α) interruption is equal to the maximum boundary of the sag disturbance.

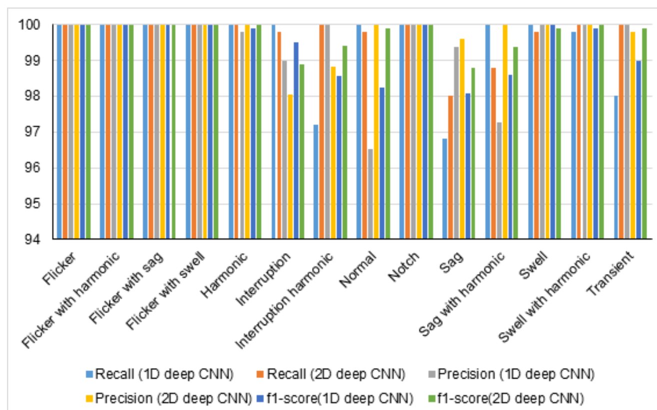

Figure 8: Bar chart of the testing evaluation between the 1D and 2D deep CNN X

As presented in Table 9 and Figure 9, generally, the value of the parameters of the 2D-X model exhibits better performance than the 1D deep CNN. The 2D deep CNN X model obtains 99.96% for the accuracy. The precision is acquired at 99.73%. The recall and f1-score reach 99.72% each. In addition, the size of the dataset and the model file are small. However, the 2D deep CNN X model takes relatively a cost computation time in training stage.

Furthermore, we verified the robustness of our approach in comparison to the previous approaches. An evaluation of the classification performance of the models using the 2D datasets from our approach and approaches used in the previous research is given in Table 10 and Figure 10. The experiment's result demonstrated that the 2D deep CNN Y model obtains 99.88% for accuracy, 99.19% for precision, 99.18% for recall, and 99.18% for f1-score. The 2D deep CNN Z reaches 99.74% for accuracy, 98.80% for precision, 97.81 for recall, and 98.25 for f1-score. It can be seen that our proposed approach outperforms other methods with 99.96% for accuracy, 99.73%

Table 8: Model performance of the 1D deep CNN (1D) and 2D deep CNN X (2D)

Disturbance categories	Recall (%)		Precision (%)		f1-score (%)	
	1D	2D	1D	2D	1D	2D
Flicker	100	100	100	100	100	100
Flicker with harmonic	100	100	100	100	100	100
Flicker with sag	100	100	100	100	100	100
Flicker with swell	100	100	100	100	100	100
Harmonic	100	100	99.8	100	99.9	100
Interruption	100	99.8	99	98.03	99.5	98.9
Interruption harmonic	97.2	100	100	98.81	98.58	99.4
Normal	100	99.8	96.52	100	98.23	99.89
Notch	100	100	100	100	100	100
Sag	96.8	98	99.38	99.59	98.07	98.79
Sag with harmonic	100	98.8	97.27	100	98.61	99.39
Swell	100	99.8	100	100	100	99.89
Swell with harmonic	99.8	100	100	100	99.89	100
Transient	98	100	100	99.8	98.98	99.9

Table 9: Summary of the models performance between the 1D and the 2D deep CNN

Parameters	1D deep CNN	2D deep CNN X
Accuracy (%)	99.91	99.96
Precision (%)	99.42	99.73
Recall (%)	99.41	99.72
F1-score (%)	99.41	99.72
Time training per epoch (second)	16	30
Model size (MB)	1.24	0.80
File size (MB)	663	128

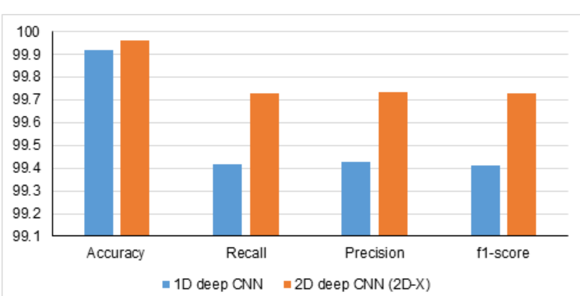

Figure 9: Bar chart of the testing evaluation between the 1D deep CNN and the 2D deep CNN X models

for precision, 99.72% for recall, and 99.72% for f1-score. It indicates that the ability of the 2D deep CNN X model which uses the dataset from our approach to identifying all the relevant disturbances within the dataset is better than the others. In addition, the capability of this model to detect only the disturbances of interest in the dataset is also higher than the previous methods. However, the computation time of our approach is still high with 30 seconds per epoch compared with the other methods. The reason is that the 2D image size resulting from our approach is a large than the previous approaches.

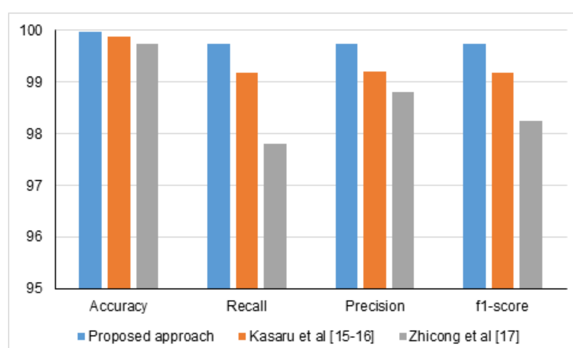

Figure 10: Bar chart of the testing evaluation between our approach and the existing methods

The results of the experiments indicate that the 2D deep CNN model using the 2D image dataset obtained from our approach increases the effectiveness of classification. The signal to image conversion using our approach boosts the 2D deep CNN performance in the PSDs classification, although the computation time is high in a training phase.

Table 10: The testing evaluation between our approach and the existing methods

Parameters	Model with the dataset using the conversion method of		
	Kasaru *et al.* [9,10]	Zhicong *et al.* [25]	Proposed approach
Accuracy (%)	99.88	99.74	99.96
Precision (%)	99.19	98.80	99.73
Recall (%)	99.18	97.81	99.72
F1-score (%)	99.18	98.25	99.72
Time training per epoch (second)	15	16	30

4 Conclusions

A robust signal to the 2D image conversion and analysis of the PSDs classification based on the 2D deep CNN is presented in this study. In data preprocessing phase, the signal is converted to the 2D grayscale image. The 2D grayscale image preserves the information and sinusoidal waveform of the signal. The conversion results are then utilized as the 2D dataset in the training and testing phase of the model. The experiment's result shows that the accuracy, the recall, and the precision values of the model are 99.96%, 99.72%, and 99.73%, respectively. These result demonstrates that our proposed approach can improve the efficacy of the PSDs classification. In addition, the performance of the proposed approach is better compared to the 1D deep CNN and the previous existing approaches. For a future study, the dataset with noise will be implemented to the 1D and 2D deep CNN model.

Acknowledgments

The authors gratefully acknowledge the helpful comments and suggestions of the reviewers for improving the presentation.

References

[1] A. Aggarwal, N. Das, M. Arora, M. M. Tripathi, "A novel hybrid architecture for classification of power quality disturbances," in *6th International Conference on Control, Decision and Information Technologies (CoDIT'19)*, pp. 1829-1834, 2019.

[2] A. Bagheri, M. H. J. Bollen, I. Y.H. Gu, "Improved characterization of multi-stage voltage dips based on the space phasor model," *Electric Power Systems Research*, vol. 154, pp. 319-328, Jan. 2018.

[3] A. Bagheri, I. Y. H. Gu, M. H. J. Bollen, E. Balouji, "A robust transform-domain deep convolutional network for voltage dip classification," *IEEE Transactions on Power Delivery*, vol. 33, no. 6, pp. 2794-2802, Dec. 2018.

[4] E. Balouji, O. Salor, "Classification of power quality events using deep learning on event images," in *3rd International Conference on Pattern Recognition and Image Analysis (IPRIA'17)*, pp. 216-221, 2017.

[5] S. S. Berutu, Y. C. Chen, "Power quality disturbances classification based on wavelet compression and deep convolutional neural network," in *International Symposium on Computer, Consumer and Control (IS3C'20)*, pp. 327-330, 2020.

[6] K. Cai, W. Cao, L. Aarniovuori, H. Pang, Y. Lin, G. Li, "Classification of power quality disturbances using wigner-ville distribution and deep convolutional neural networks," *IEEE Access*, vol. 7, pp. 119099-119109, Aug. 2019.

[7] IEEE, *IEEE Recommended Practice for Monitoring Electric Power Quality* 2009: c1-81, IEEE 1159.

[8] R. Igual, C. Medrano, F. J. Arcega, G. Mantescu, "Integral mathematical model of power quality disturbances," in *18th International Conference on Harmonics and Quality of Power (ICHQP'18)*, Ljubljana, pp. 1-6, 2018.

[9] S. Karasu, Z. Saraç, "Investigation of power quality disturbances by using 2D discrete orthonormal S-transform, machine learning and multi-objective evolutionary algorithms," *Swarm Evolutionary Computation*, vol. 44, pp. 1060-1072, Feb. 2019.

[10] S. Karasu, Z. Saraç, "Classification of power quality disturbances by 2D-Riesz Transform, multi-objective grey wolf optimizer and machine learning methods," *Digital Signal Processing*, vol. 101, June 2020.

[11] P. Khetarpal, M. M. Tripathi, "A critical and comprehensive review on power quality disturbance detection and classification," *Sustainable Computing: Informatics and Systems*, vol. 28, Dec. 2020.

[12] S. Kiranyaz, O. Avci, O. Abdeljaber, T. Ince, M. Gabbouj, D. J. Inman, "1D convolutional neural networks and applications: A survey," *Mechanical Systems and Signal Processing*, vol. 151. Apr. 2021.

[13] H. Liu, F. Hussain, Y. Shen, S. Arif, A. Nazir, M. Abubakar, "Complex power quality disturbances classification via curvelet transform and deep learning," *Electric Power Systems Research*, vol. 163, pp. 1-9. Oct. 2018.

[14] S. K. G. Manikonda, S. Gangwani, S. P. K. Sreckala, J. Santhosh, D. N. Gaonkar, "Power quality event classification using convolutional neural networks on images," in *IEEE 1st International Conference on*

Energy, Systems and Information Processing (ICESIP'19), Chennai, India, pp. 1-5, 2019.

[15] N. Mohan, K. P. Soman, R. Vinayakumar, "Deep power: Deep learning architectures for power quality disturbances classification," in *International Conference on Technological Advancements in Power and Energy (TAP Energy'17)*, pp. 1-6, 2017.

[16] Ş. Öztürk, B. Akdemir, "Cell-type based semantic segmentation of histopathological images using deep convolutional neural networks," *International Journal of Imaging Systems and Technology*, vol. 29, pp. 234-246, Feb. 2019.

[17] Y. Shen, M. Abubakar, H. Liu, F. Hussain, "Power quality disturbance monitoring and classification based on improved PCA and convolution neural network for wind-grid distribution systems," *Energies*, vol. 12, no. 7, pp. 1280, Apr. 2019.

[18] H. Sindi, M. Nour, M. Rawa, Ş. Öztürk, K. Polat, "A novel hybrid deep learning approach including combination of 1D power signals and 2D signal images for power quality disturbance classification," *Expert Systems with Applications*, vol. 174, July 2021.

[19] A. Tharwat, "Classification assessment methods," *Applied Computing and Informatics*, vol. 17, no. 1, pp. 168-192, Jan. 2021.

[20] J. Wang, Z. Xu, Y. Che, "Power Quality Disturbance Classification Based on Compressed Sensing and Deep Convolutional Neural Networks," *IEEE Access*, vol. 7, pp. 78336-78346, Jun. 2019.

[21] S. Wang, H. Chen, "A novel deep learning method for the classification of power quality disturbances using deep convolutional neural network," *Applied Energy*, vol. 235, pp. 1126–1140, Feb. 2019.

[22] F. Xiao, T. Lu, M. Wu, Q. Ai, "Maximal overlap discrete wavelet transform and deep learning for robust denoising and detection of power quality disturbance," *IET Generation, Transmission & Distribution*, vol. 14, pp. 140-147, Jan. 2020.

[23] J. Xu, Y. Zhang, D. Miao, "Three-way confusion matrix for classification: A measure driven view," *Information Sciences*, vol. 507, pp. 772-794, Jan. 2020.

[24] H. Xue, A. Chen, D. Zhang, C. Zhang, "A novel deep convolution neural network and spectrogram based microgrid power quality disturbances classification method," in *IEEE Applied Power Electronics Conference and Exposition (APEC'20)*, New Orleans, LA, USA, pp. 2303-2307, 2020.

[25] Z. Zheng, L. Qi, H. Wang, A. Pan, J. Zhou, "Recognition method of voltage sag causes based on two-dimensional transform and deep learning hybrid model," *IET Power Electronics*, vol. 13, pp. 168-177. Jan. 2020.

Biography

Yeong-Chin Chen received the M.S. and Ph.D. degrees in electrical engineering from National Cheng Kung University, Tainan City in 1989 and 1998, respectively. He worked with the Marine Science and Technology Center, Underwater Technology Department, the National Chung Shan Institute of Science and Technology, Taoyuan from 1989 to 2000, as a senior researcher. He conducted research on sonar system design and sound technology. He is currently a professor in computer science and information engineering with Asia University, Taichung. His research interests include acoustical transducer engineering, power signal measurement & analysis, automatic measurement, and software engineering. In recent years, his research has also been focused on smart power meters implemented in the internet of things (IoT) platforms for big-data power saving management applications & Power Quality monitor technology.

Sunneng Sandino Berutu received the B.S. degree in computer science from Immanuel Christian University, Yogyakarta in 2000 and the M.S. degree in information system from University of Diponegoro, Semarang in 2013. He is currently pursuing the Ph.D. degree at Department of Computer Science and Information Engineering, Asia University, Taichung. He is an Information and Technology lecturer at Immanuel Christian University, Yogyakarta, Indonesia. His research interest mainly focused on IoT and power quality.

Long-Chen Hung was born in Kaohsiung, Taiwan, in 1973. He received the M.S. degree from the electrical engineering of I-Shou University, Kaohsiung, in 1998 and the Ph.D. degree from the electrical engineering of Nation Central University, Chungli, in 2005. He is currently an assistant professor in the Department of Electronic Engineering, Lungh-Wa University of Science and Technology. His research interests include deep learning, reinforcement learning, signal processing, control system and AIoT with power quality.

Mariana Syamsudin Mariana Syamsudin is a Ph.d student in Department of Computer Science and Information Engineering Asia University, Taiwan. She earned her bachelor degree in Electrical Engineering from Tanjungpura University, Indonesia and her master degree from Bandung Institute of Technology (ITB), Indonesia. She is an Information and Technology lecturer at Polytechnic State of Pontianak, Indonesia. Her research interest focus on reinforcement learning model.